Reaction Chemistry & Engineering

ROYAL SOCIETY OF CHEMISTRY

PAPER

Published on 06 July 2026

Cite this: DOI: 10.1039/d6re00193a

Performance of Pt-based catalysts in perhydro benzyltoluene dehydrogenation: from semi-batch screening to continuous operation

Elisabeth Herzinger, [a] Jona Berger,[a] Nicolas Patrick Johner,[b] Franziska Auer [b] and Moritz Wolf *[ac]

Standardised semi-batch testing is widely used for catalyst screening in liquid organic hydrogen carrier (LOHC) dehydrogenation. However, literature on their quantitative transferability to continuous reactor operation is scarce. This study investigates the dehydrogenation of perhydro benzyltoluene (H12-BT) over three Pt-based (PtRe, Pt and PtS) alumina-supported catalysts in a three-phase stirred tank slurry reactor, comparing the results with those from semi-batch tests at comparable operating parameters and degrees of dehydrogenation. Across the investigated temperature range of 210–250 °C, semi-batch operation yielded a substantially higher absolute hydrogen productivity than continuous stirred tank reactor (CSTR) operation, exceeding steady-state values by a factor of three to five. At the same time, the order of catalyst productivity was preserved across reactor concepts: PtRe > Pt > PtS. Logarithmic, ratio and parity analyses revealed that the deviation is systematic rather than random and can be approximated by a reactor dependent empirical transfer factor. However, the degree of quantitative transferability remains catalyst dependent. Apparent Arrhenius analyses revealed comparable activation energies for both reactor concepts but lower pre-exponential factors for CSTR operation. This indicates that the CSTR primarily shifts the attainable rate level rather than the apparent temperature sensitivity. Further, liquid phase analysis showed that both reactor concepts follow the same primary dehydrogenation pathway. However, continuous operation results in enrichment of the partially dehydrogenated H6-BT intermediate. The results demonstrate that semi-batch screening is suitable for preselecting and ranking catalysts, but evaluating the quantitative process for continuous LOHC dehydrogenation requires reactor specific correction.

Received 24th May 2026,
Accepted 3rd July 2026

DOI: 10.1039/d6re00193a

rsc.li/reaction-engineering

1. Introduction

Liquid organic hydrogen carriers (LOHCs) have emerged as a promising solution for safe and efficient hydrogen storage and transport.[1–4] This technology addresses one of the key challenges in a hydrogen economy: the need for practical, scalable, and safe methods to store and distribute hydrogen, thereby supporting global decarbonisation efforts and the transition to sustainable energy systems.[5,6] By chemically binding hydrogen to organic molecules, LOHCs enable storage in liquid phase under ambient conditions, which simplifies handling and logistics.[2] Among the various LOHC candidates, benzyltoluene (BT) is particularly attractive for large-scale deployment due to its commercial availability, low toxicity, high chemical stability, low vapor pressure, and favourable hydrogen storage capacity.[7–9]

The performance of LOHC dehydrogenation systems is strongly influenced by the choice of catalyst, with Pt-based catalysts being commonly used in high performance systems.[10–12] Numerous studies have focused on optimising catalysts with key strategies including selective poisoning of low coordinated sites,[13–19] choice of alternative support materials,[16,20–27] alumina support modification,[17,28–37] particle size control,[18,26,27,32,38–42] and promoter addition.[19,33–37,42–50] Most of these investigations are predominantly conducted in batch or semi-batch reactor systems (Fig. 1, Table S1), which offer defined conditions and enable rapid screening of catalyst performance. Continuous studies have mainly focused on gas phase dehydrogenation of methylcyclohexane to toluene, while liquid phase dehydrogenation is commonly realised in semi-batch operation mode. As a result, catalyst development in this

[a] Karlsruhe Institute of Technology (KIT), Institute of Catalysis Research and Technology, Hermann-von-Helmholtz-Platz 1, 76344 Eggenstein-Leopoldshafen, Germany. E-mail: moritz.wolf@kit.edu
[b] Forschungszentrum Jülich GmbH, Helmholtz Institute Erlangen-Nürnberg for Renewable Energy (IET-2), Cauerstraße 1, 91058 Erlangen, Germany
[c] Karlsruhe Institute of Technology (KIT), Engler-Bunte-Institut, Engler-Bunte-Ring 1, 76131 Karlsruhe, Germany

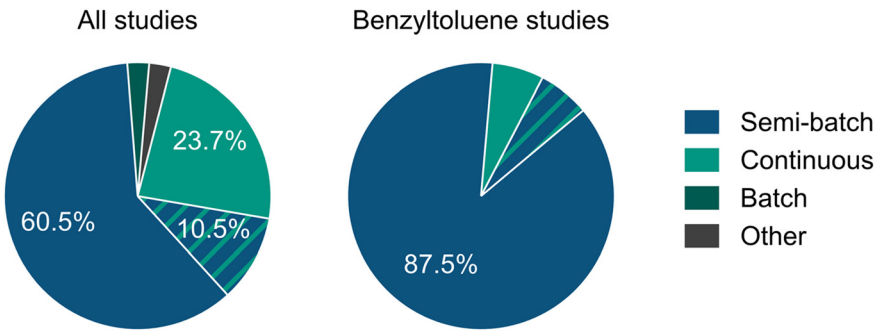

Fig. 1 Operation modes in literature studies for Pt-based LOHC dehydrogenation catalyst development (Table S1). Only studies with a primary focus on catalyst development or catalyst optimisation are included, *i.e.* studies primarily focused on reactor design or process operation were not considered. Left: all studies included in the literature survey (N = 38): semi-batch only, n = 23 (60.5%); continuous only, n = 9 (23.7%); mixed semi-batch/continuous operation or continuous validation, n = 4 (10.5%), shown as the hatched segment; batch only, n = 1 (2.6%); and other/not applicable, n = 1 (2.6%). Right: benzyltoluene studies, referring to perhydro benzyltoluene/benzyltoluene (H12-BT / H0-BT); (N = 16): semi-batch only, n = 14 (87.5%); continuous only, n = 1 (6.3%); mixed semi-batch/continuous operation or continuous validation, n = 1 (6.3%); batch only, n = 0 (0%); and other/not applicable, n = 0 (0%).

field largely relies on semi-batch experiments to identify promising materials.

Technical hydrogen release processes are usually carried out in continuously operated reactors,[51] where the reaction environment differs fundamentally from semi-batch operation in the lab environment. Continuous systems are characterised by feed and withdrawal of the reaction mixture, leading to residence time distributions and steady-state compositions, which can influence the apparent driving force for dehydrogenation under operating conditions.[52,53] Semi-batch operation follows a transient composition trajectory, whereas continuous stirred-tank operation reaches a steady-state composition after sufficient residence time (Fig. 2). Reactor configuration may therefore influence the observed catalyst performance even when temperature, catalyst loading, and overall reaction window are otherwise comparable. Although it is often assumed that catalysts that perform well in batch experiments perform

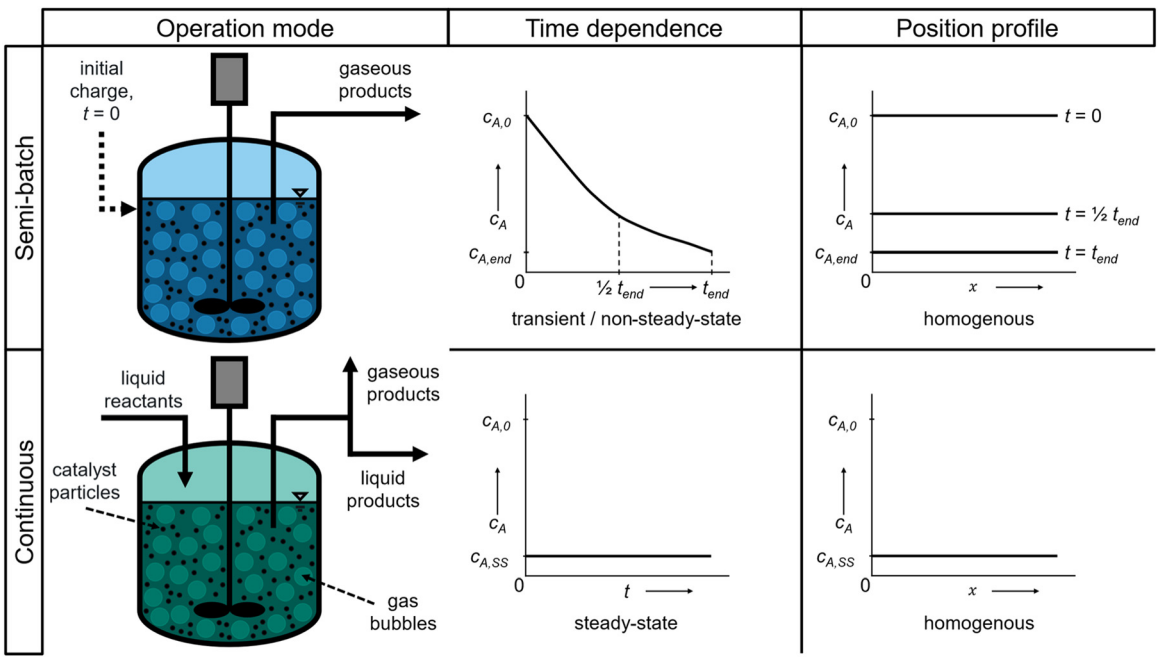

Fig. 2 Conceptual comparison of semi-batch and continuous stirred tank operation for catalytic testing in LOHC dehydrogenation. In both operation modes, liquid reactants are contacted with suspended catalyst particles under agitation, forming a gas–liquid–solid slurry. In the semi-batch reactor, the liquid reactants and catalyst are initially charged at t = 0, while gaseous products leave the reactor. The liquid phase concentration therefore changes with time, resulting in transient, non-steady-state operation. In the continuous reactor, liquid reactants are continuously fed and gaseous and liquid products are continuously withdrawn. After reaching steady-state, the concentration remains constant with time. For both schematics, ideal mixing is assumed, resulting in homogeneous concentrations throughout the reactor volume at a given time.

similarly under continuous conditions, there is a lack of systematic investigations justifying the simple transfer of catalyst performance to a technical environment.

Recent studies have shown that apparent dehydrogenation performance can strongly depend on reactor configuration through changes in hydrogen partial pressure and the corresponding conversion, LOHC concentration or the general effect of dilution, and transport or contacting limitations under continuous operation.[54–56] These effects may alter the accessible degree of dehydrogenation (DoD) and, therefore, the observed productivity. At the same time, reactor induced differences are not necessarily associated with a change in the underlying reaction chemistry, but may instead reflect that different reactor concepts probe different positions along the same dehydrogenation pathway. Addressing this distinction is essential for understanding how catalyst screening results translate to realistic process conditions.

Among the catalysts reported for perhydro benzyltoluene dehydrogenation, the bimetallic PtRe system described by Strauch *et al.*[48] demonstrated superior performance when compared to a monometallic Pt catalyst. The Re-promoted catalyst exhibited faster initial hydrogen release and significantly higher productivity at low DoDs. This enhanced performance was attributed to platinum being structurally promoted by rhenium, resulting in smaller platinum particles, higher dispersion and accelerated conversion of partially dehydrogenated intermediates.

In this work, the dehydrogenation of perhydro benzyltoluene (Fig. S1) is investigated over Al_2O_3-supported PtRe, Pt and PtS catalysts in a continuous three-phase stirred tank slurry reactor and compared with corresponding semi-batch data. It should be noted that the continuous stirred tank reactor (CSTR) investigated in this work is not intended to directly represent industrial LOHC dehydrogenation reactors, which are typically operated in plug-flow configurations, but rather serves as a well-defined continuous system to assess reactor dependent effects on catalyst performance. The CSTR configuration is of particular interest for LOHC dehydrogenation because the use of finely dispersed catalyst particles and intensive mixing can provide favourable heat and mass transfer as well as near-isothermal operation under strongly endothermic conditions.[55] As a benchmark, the commercially available PtS/Al_2O_3 catalyst (Elemax D) represents the reference system for technical BT-based LOHC dehydrogenation plants. The three selected catalysts provide a suitable basis for studying transferability of performance data across reactors as they differ in composition and expected catalytic performance, while at the same time representing the current commercial state of the art and two well defined research catalysts that have previously been evaluated under semi-batch conditions. By systematically comparing absolute productivity, scaling behaviour, parity relations, apparent kinetics, and liquid phase composition at comparable DoDs, this work assesses the reliability of semi-batch screening for prediction of catalyst performance during CSTR operation. In this way, the study aims to establish a process-oriented framework for translating catalyst screening results into realistic expectations for continuous hydrogen release.

2. Experimental

2.1. Materials

Chloroplatinic acid hydrate ($H_2[PtCl_6]$, ≥99.9% trace metal basis, platinum content 37–40%) and rhenium(VII) oxide (Re_2O_7, ≥99.9% trace metal basis, rhenium content 75.7–78.0%) were purchased from Sigma Aldrich. These chemicals were used as received. Boehmite (PURAL TH300) was provided by Sasol Germany and heated to 550 °C for 3 h in a muffle furnace under ambient atmosphere to yield alumina. A commercial PtS egg–shell catalyst (EleMax D; 2–4 mm spheres; Clariant Produkte GmbH) was supplied by Hydrogenious LOHC Technologies (Germany), while the corresponding shaped Al_2O_3 support (shaped Al_2O_3 carrier spheres) was provided from Clariant Produkte GmbH and ground and sieved into particle size fraction <125 μm. Fully hydrogenated perhydro benzyltoluene (H12-BT) was purchased from Hydrogenious LOHC Technologies (Germany) and contained minor impurities of benzyltoluene (H0-BT) and partially hydrogenated benzyltoluene (H6-BT), resulting in a degree of hydrogenation (DoH) of 99.7% (Fig. S2) corresponding to a DoD of 0.3%. Argon (ALPHAGAZ 2, quality 6.0, >99.9999 mol%) was purchased from Air Liquide.

2.2. Catalyst preparation

Three catalysts were used in this study. These included a commercial platinum-based catalyst with selective sulphur poisoning (PtS) and two impregnated catalysts: platinum–rhenium (PtRe) and platinum (Pt). The commercial PtS catalyst was ground and sieved into a particle size range of 63–125 μm. PtRe and Pt catalysts were synthesised using calcined PURAL TH300 support following a procedure reported by Strauch *et al.*[48] based on wet impregnation using ion adsorption. A precursor solution was prepared in ultrapure water containing $H_2[PtCl_6]$ and optional Re_2O_7, targeting a platinum concentration of 0.05 wt%. The required amount of alumina powder was added to the solution after 10 min stirring to obtain a platinum loading of 0.3 wt% and an additional rhenium loading of 0.15 wt% for the bimetallic PtRe catalyst. Stirring of the solution for 10 min was followed by solvent removal in a rotary evaporator at 50 °C. Drying was carried out under a stepwise reduced pressure (140–20 mbar) over 3 h, followed by calcination in a Nabertherm L9/11 muffle furnace at 400 °C for 4 h in air. The reduction of the catalyst was performed *via* thermal treatment in a horizontal tube furnace (PMA, controller: KS 98-1). A heating rate of 10 °C min^{-1} under argon flow was applied. Once the target reduction temperature of 400 °C was reached and stabilised, argon was replaced with 500 ml min^{-1} forming gas (10 vol%

H_2 in N_2) to initiate reduction. After 2 h of reduction, the catalyst powder was cooled under argon flow. In this study, the use of finely powdered catalysts minimises internal mass transfer limitations and differs from the shaped catalysts typically employed in industrial reactors. Consequently, the absolute performance values reported here are not directly transferable to technical systems without considering diffusion and transport effects associated with catalyst geometry.

2.3. Material characterisation

X-ray diffraction (XRD) of the support materials and the catalysts was conducted using a PANalytical X'Pert Pro diffractometer with Cu Kα radiation (λ = 0.154060 nm). Measurements were carried out over a 2θ range from 5° to 80° at room temperature, with a scan rate of approx. 0.01° s^{-1} and a total measurement time of 2 h. For phase identification, reference patterns of γ-Al_2O_3 (COD-ID: 2107301), θ-Al_2O_3 (COD-ID: 1200005) and α-Al_2O_3 (COD-ID: 2101052) were used.

The salt addition method was applied, to determine the pH at point of zero charge (pH_{PZC}) of the support materials.[57–59] Approx. 0.05 g of solid sample was weighed into 20 ml vials, followed by the addition of about 10 g of 0.1 M $NaNO_3$ solution with pH values between 3 and 10 at pH intervals of one using 0.1 M HNO_3 and 0.1 M NaOH. The initial pH (pH_i) was measured with a pH electrode (Mettler Toledo Seven Compact). The samples were shaken for 24 h at 300 rpm and 25 °C. After filtration, the final pH (pH_f) of the solutions was measured. The pH change (ΔpH) was calculated, and pH_{PZC} was obtained from the intersection of the ΔpH *versus* pH_i curve with the *x*-axis.

Structural characterisation of the calcined alumina support was performed *via* nitrogen physisorption using a NOVA 2000 (Quantachrome Instruments). Prior to analysis, 100–300 mg of sample was degassed at 130 °C for 20 h. The pore size distribution was assessed by applying the BJH method using the desorption branch of the isotherm, while the specific surface area was calculated using the BET method over a relative pressure (p/p_0) range of 0.05–0.30.

Catalyst metal loading was determined by inductively coupled plasma atomic emission spectrometry (ICP-AES, Agilent 725, Agilent Technologies, Inc.). For this, 20–50 mg of catalyst was digested in 8 ml of a HCl–HNO_3 mixture (1 : 3 volumetric ratio) using microwave-assisted decomposition. Platinum concentrations were quantified at a characteristic wavelength of 214.424 nm, while Re concentrations were determined at 197.248 and 227.525 nm.

CO pulse chemisorption was used to probe the accessible active sites for Pt-based catalysts. Approx. 200–400 mg of the respective catalyst was analysed using an Autochem III (Micromeritics). Prior to each measurement the samples were dried at 120 °C under helium. All materials were reduced *in situ* under 10 vol% H_2/Ar at 400 °C for 60 min. The sample was then cooled down to 35 °C and flushed with a continuous flow of He. Next, the sample was probed with intermittent CO/He pulse dosing. Each pulse corresponded to an injected gas volume of approx. 0.54 ml (10.05% CO in He). The pulses were repeated every two minutes until no further uptake was observed, indicating saturation of the catalyst surface.

2.4. Continuous reactor setup and experimental procedure

Continuous catalytic dehydrogenation of perhydro benzyltoluene was performed in a CSTR with a 450 ml pressure vessel, mechanical stirring, and electrical heating (Parr Instrument, Fig. S3). The system features a continuous LOHC feed provided *via* an HPLC pump, mass flow controllers (Bronkhorst) connected to a gas inlet, and product removal *via* a two-phase outlet connected to a gas–liquid separation unit with a cooled condenser and buffer tank. An autosampler at the liquid outlet of the buffer tank enables liquid sampling while hydrogen in the gas phase product stream is quantified in-line using a thermal conductivity detector (TCD). A detailed description of the experimental setup has been reported previously.[55]

A set of standard operating parameters was selected for all dehydrogenation experiments (Table 1). Before each experiment, 250 ml of H12-BT were loaded into the reactor as the working reaction volume was previously shown to be approx. 270 ml.[55] Additional H12-BT was fed at a rate of 2.0 ml min^{-1} while flowing 200 ml min^{-1} of argon as sweep gas until the pneumatic on–off valve opened and closed periodically. Subsequently, the H12-BT feed was stopped, the dehydrogenation catalyst was added, and the system was purged again with 200 ml min^{-1} of argon until a stable signal was obtained for the thermal conductivity detector. Heating was initiated alongside the gas flow and stirring. The H12-BT feed and automated sampling were started simultaneously, once the temperature in the reactor reached 230 °C. After reaching the target temperature of 250 °C, the reactor was operated under steady-state conditions for five hours. The temperature was then varied stepwise, with each setpoint maintained for at least four hours.

2.5. Semi-batch laboratory catalyst screening

Based on the semi-batch study reported by Strauch *et al.*,[48] the PtRe and Pt data were taken as reference values, while

Table 1 Standard operation parameters for the dehydrogenation of perhydro benzyltoluene in a continuous three-phase stirred tank slurry reactor

Parameter	Value
Pressure/bar_a	1.0
Temperature/°C	250, 240, 230, 220, 210
Stirrer speed/rpm	1000
Catalyst amount/g	7.16
Liquid feed/ml min^{-1}	2.0
Ar flow/ml_N min^{-1}	200

the commercial PtS catalyst was tested in this work using the same procedure. The dehydrogenation experiments were conducted in a 100 ml round bottom glass flask setup equipped with a reflux condenser and a heating mantle (Fig. S4). A magnetic stirring bar was used to ensure mixing, while the liquid phase temperature was monitored using a type K thermocouple with the tip being immersed in the reaction liquid and controlled by a temperature controller. Before each experiment, the H12-BT equivalent of 2 g reversibly bound H_2 (32.2 g H12-BT) was added to the flask and the catalyst amount was adjusted to a fixed molar ratio of H12-BT to platinum of 10^{-4} mol_{Pt} $mol_{H12\text{-}BT}^{-1}$. The catalyst (1.078 g) was placed in a stainless-steel addition device, allowing its introduction under reaction conditions without opening the system. A constant flow of 200 ml_N min^{-1} argon was supplied by a mass flow controller to inertise the system and to serve as sweep gas for the released hydrogen during the experiment. The reactor contents were heated to the target temperature (210, 220, 230, 240 and 250 °C), while stirring continuously. Once the desired temperature was reached and stabilised, the catalyst was added to initiate the reaction. The experiments were performed under ambient pressure for a reaction time of 1320 min, while liquid samples were withdrawn at defined time intervals for compositional analysis. The hydrogen concentration of the off-gas was continuously measured with a TCD.

2.6. Analysis of liquid samples

Liquid samples obtained during the dehydrogenation experiments were analysed using an Agilent 8890 gas chromatograph equipped with a DB-17 ms column (30 m × 250 μm) and flame ionisation detection (GC-FID). Approx. 100 μl of each sample was diluted in 0.9 ml of isopropanol and 1 μl of the resulting solution was injected and analysed using a predefined temperature programme (Table S2).

The GC-FID enables distinct separation of the individual BT species, including H12-BT, H6-BT, H0-BT and the major by-product methylfluorene (Fl).[7] The resulting chromatographic data were processed using Python, and quantification was based on the integrated peak areas. From these, the mole fractions of the individual H*x*-BT species $x_{Hx\text{-}BT}$ were determined and subsequently used to calculate the degree of dehydrogenation according to GC (DoD_{GC}) with eqn (1).

$$DoD_{GC} = \left(1 - \left[\frac{12}{12}\cdot x_{H12\text{-}BT} + \frac{6}{12}\cdot x_{H6\text{-}BT} + \frac{0}{12}\cdot(x_{H0\text{-}BT} + x_{Fl})\right]\right)\cdot 100\% \quad (1)$$

2.7. General performance metrics

The precious metal-based catalyst productivity (Prod.) relates the mass of released hydrogen m_{H_2} per unit of time Δt to the mass of catalytically active platinum m_{Pt} during dehydrogenation experiments. It can be determined according to eqn (2) based on the volumetric flow of hydrogen out of the reactor $\dot{V}_{H_2}$, quantified using the pre-calibrated in-line TCD, the catalyst mass $m_{cat.}$, the platinum loading w_{Pt}, and the density of hydrogen ρ_{H_2} (0.0898 kg m^{-3} at 273.15 K and 100 kPa).[60] During semi-batch operation, the hydrogen release at certain DoD levels reflecting the steady-state operation in the CSTR were considered.

$$\text{Prod.} = \frac{m_{H_2}}{m_{Pt}\cdot\Delta t} = \frac{\dot{V}_{H_2}\cdot\rho_{H_2}}{w_{Pt}\cdot m_{cat.}} \quad (2)$$

The platinum-based turnover frequency (TOF) expresses the number of molecules formed per active site and unit time.[53,61] Accordingly, it can be defined as the molar rate of hydrogen formation $\dot{n}_{H_2}$ normalised to the number of surface-accessible platinum sites, which is derived from the total molar amount of platinum n_{Pt} and the fraction of exposed platinum atoms. Using the platinum-based productivity, the platinum dispersion D_{Pt}, and the molar mass of platinum M_{Pt} (195.08 g mol^{-1})[62] and hydrogen M_{H_2} (2.016 g mol^{-1}),[60] the TOF can be approximated *via* eqn (3).

$$\text{TOF} = \frac{\dot{n}_{H_2}}{n_{Pt}\cdot D_{Pt}} = \frac{\text{Prod.}\cdot M_{Pt}}{M_{H_2}\cdot D_{Pt}} \quad (3)$$

2.8. CSTR specific definitions

The variables and models used for the CSTR evaluation are defined in this section. Further details on the mathematical derivation can be found in a previous study.[55]

To account for variations in hydrodynamic conditions, the experimental results from continuous operation were analysed using dimensionless time θ, defined as the ratio of the time on stream t to the mean residence time of the liquid phase in the reactor τ.[52] Herein, τ is estimated as the ratio of the liquid holdup under reaction conditions V_R (CSTR: ~270 ml), to the volumetric flow rate of H12-BT $\dot{V}_{H12\text{-}BT}$ (eqn (4)). The reactor stability during continuous operation was assessed using the relative change in productivity over dimensionless time $\Delta\text{Prod.}(\theta)$ as a steady-state indicator.

$$\theta = \frac{t}{\tau} = t\frac{\dot{V}_{H12\text{-}BT}}{V_R} \quad (4)$$

As a measure for the volumetric productivity of the reactor during continuous operation, the space–time yield (STY) was determined by relating the molar flow of products $\dot{n}$ to the reaction volume V.[53] Calculation was performed according to eqn (5) using the volumetric hydrogen flow rate $\dot{V}_{H_2}$, the liquid holdup under reaction conditions V_R, and conversion of the volumetric flow into a molar flow using the molar gas volume under standard conditions V_m (22.4 l mol^{-1}).[63]

$$\text{STY} = \frac{\dot{n}}{V} = \frac{\dot{V}_{H_2}}{V_m V_R} \quad (5)$$

Assuming ideal backmixing and a constant liquid reaction volume, the DoD can also be determined from the quantified flow of released hydrogen according to the TCD (DoD_{TCD}) during continuous operation. For this purpose, a virtual concentration of hydrogenated BT equivalents $c_{Hx\text{-}BT}$ at the reactor outlet is derived over time t from the released hydrogen using a molar material balance. Normalising $c_{Hx\text{-}BT}$ to the inlet concentration of H12-BT $c_{H12\text{-}BT}$ yields the DoD_{TCD} as expressed in eqn (6).

$$DoD_{TCD}(t) = \left(1 - \frac{c_{Hx\text{-}BT}(t)}{c_{H12\text{-}BT}}\right) \cdot 100\% \quad (6)$$

Conversion X refers to the relative decrease in the molar quantity of a component during reaction. For dehydrogenation during continuous operation, the conversion is evaluated from the difference in reversibly bound hydrogen between the H12-BT feed and the liquid product stream at the reactor outlet. If the feed is fully hydrogenated the dehydrogenation conversion X_{DoD} can be approximated by the DoD with eqn (7).

$$X_{DoD} \approx \frac{DoD}{100\%} \quad (7)$$

To assess thermodynamic limitations, the equilibrium conversion X_{eq} was calculated using the equilibrium degree of hydrogenation of benzyltoluene $DoH_{eq,BT}$ reported by Rüde *et al.*[7] according to eqn (8).

$$X_{eq}(T,p) = 1 - DoH_{eq,BT}(T,p) \quad (8)$$

2.9. Effective kinetic model

Kinetic parameters were estimated with a simplified model based on the concentration of hydrogenated BT equivalents $c_{Hx\text{-}BT}$ to account for the dependence of the reaction rate on the concentration of available reactants. The effective formation rate of hydrogen $r_{H_2,eff}$ was calculated from the measured productivity and the molar mass of hydrogen M_{H_2}, including the corresponding conversion of units. Applying the stochiometric relationship of the H12-BT dehydrogenation (release of six moles of hydrogen per H12-BT for complete dehydrogenation), $r_{H_2,eff}$ can also be expressed *via* the effective rate constant k_{eff}, the concentration of hydrogenated BT equivalents $c_{Hx\text{-}BT}$, and the effective reaction order n_{eff} (eqn (9)). This formulation is intended as an effective reactor scale description and does not represent intrinsic species resolved kinetics.

$$r_{H_2,eff} = \text{Prod.} \frac{1}{M_{H_2}} \frac{1000\ g_{Pt}}{1\ kg_{Pt}} \frac{1\ min}{60\ s} = 6 \cdot k_{eff} \cdot c_{Hx\text{-}BT}^{n_{eff}} \quad (9)$$

For evaluation of the temperature dependence, k_{eff} was determined from $r_{H_2,eff}$ assuming an apparent first-order dependence on $c_{Hx\text{-}BT}$ (n_{eff} = 1) according to eqn (10). The resulting parameter is therefore an effective rate constant combining influence of composition, intermediate formation, hydrogen inhibition, thermodynamic limitations, and possible mass transport limitations, rather than a mechanistic intrinsic constant. Its temperature dependence was described by an Arrhenius type relation, where k_0 denotes the pre-exponential factor, $E_{A,e}$ the apparent activation energy, R the universal gas constant, and T the absolute temperature.[53]

$$k_{eff}(T) = \frac{r_{H_2,eff}}{6 \cdot c_{Hx\text{-}BT}} = k_0 \cdot \exp\left[\frac{-E_{A,e}}{RT}\right] \quad (10)$$

The natural logarithm of eqn (10), as shown in eqn (11), yields a linear relationship. In the corresponding Arrhenius plot, $E_{A,e}$ and k_0 can be obtained from slope and y-axis intercept, respectively.

$$\ln(k_{eff}) = \ln(k_0) - \frac{E_{A,e}}{R}\frac{1}{T} \quad (11)$$

3. Results and discussion

3.1. Catalyst properties and structural characteristics

The catalysts and support materials were characterised to establish the structural, textural, and surface properties relevant for platinum dispersion and site accessibility (Table 2). A detailed discussion of the characterisation results can be found in the SI. XRD identified the commercial support as θ–α-Al_2O_3 and the as-prepared alumina as γ-Al_2O_3. The crystalline frameworks of both supports are retained after impregnation and thermal treatment, while no detectable diffraction peaks from platinum or rhenium are observed due to the low metal loadings and high dispersion (Fig. S5). The pH_{PZC} was determined for both supports (Fig. S6). Slightly higher values were obtained for θ–α-Al_2O_3, reflecting differences in alumina phase composition and surface properties. N_2 physisorption revealed that the γ-Al_2O_3 has a higher surface area and larger mesopores than the θ–α-Al_2O_3 (Fig. S7, Table S3). Similar adsorption–desorption behaviour before and after impregnation indicates that the pore structure remains largely accessible and intact. ICP-AES analyses confirmed comparable platinum loadings across all catalysts (Table S4). CO pulse chemisorption yielded apparent platinum dispersions of 68%, 88%, and 62% for PtRe, Pt, and PtS, respectively, indicating differences in accessible platinum surface sites (Table S5).

3.2. Continuous dehydrogenation experiments

All catalysts were studied in a three-phase stirred tank slurry reactor[55] in the temperature range of 210 to 250 °C (Fig. 3) to sustain the majority of the LOHC in the liquid phase (boiling point of isomers in the range of 264–272 °C at 1.0 bar_a)[7] enabling direct comparison with the performance from semi-batch experiments under atmospheric pressure. Following an initial spike in productivity due to the fully

Table 2 Summary of catalyst properties

Catalyst	Al_2O_3[a]	S_{BET}[b]/m^2 g^{-1}	d_{BJH}[b]/nm	pH_{PZC}[c]	Pt[d]/wt%	Re[d]/wt%	S[d]/wt%	D_{Pt}[e]/%
PtRe	γ	81	28	6.5	0.27	0.16	—	68
Pt					0.30	—	—	88
PtS	θ, α	31	21	7.1	0.24	—	0.11	62

[a] Alumina crystal phase determined by XRD. [b] Textural properties determined by N_2 physisorption: S_{BET} denotes the specific surface area calculated by the Brunauer–Emmett–Teller method, and d_{BJH} denotes the average pore diameter obtained from Barrett–Joyner–Halenda desorption method. [c] pH at the point of zero charge, determined by the salt addition method. [d] Elemental loading determined by ICP-AES. [e] Apparent platinum dispersion determined by CO pulse chemisorption, assuming adsorption of one CO molecule per accessible Pt surface atom.

hydrogenated LOHC in the reactor and liquid feed during start-up at 250 °C, a constant hydrogen release was observed for $\theta > 2$ (Fig. 3). Subsequently the reactor temperature was decreased stepwise and maintained for approx. 2θ to enable steady-state operation at each setpoint. Lower reaction temperatures resulted in the expected decrease in catalyst productivity, space–time yield, and conversion (Fig. 3, Table S6). As indicated by $\Delta Prod.(\theta)$ the reactor operates under quasi-steady-state conditions following each temperature adjustment. Although transient deviations are observed, no systematic loss of activity or progressive deactivation is evident for any of the catalysts over the investigated temperature range.

Similar to previous results using a semi-batch dehydrogenation setup,[48] the PtRe catalyst exhibited the highest hydrogen productivity across the whole tested temperature range (Fig. 3, Table S6). In line with the observed catalyst productivity trends, the highest DoD was obtained for PtRe (20.2% at 250 °C), followed by Pt (12.3%), and PtS (7.2%). When comparing PtRe to the Pt catalyst, the productivity was enhanced by 71–97% while reaching significantly higher DoD, which confirms a higher intrinsic dehydrogenation activity within the investigated temperature window. This is further supported by TOF values, which show that PtRe maintains the highest intrinsic activity when normalised to accessible platinum surface sites (Fig. S8). In contrast, Pt and PtS exhibit comparable TOFs over the investigated temperature range, indicating that the accessible Pt sites in both catalysts display similar apparent intrinsic dehydrogenation activities. Nevertheless, the PtS catalyst shows a lower overall productivity at higher reaction temperatures (Fig. 3, Table S6). This decrease is likely not only related to a reduced number of accessible Pt surface sites due to selective sulphur poisoning, as indicated by CO pulse chemisorption measurements (Table 2), but may also reflect sulphur induced electronic modification of neighbouring Pt sites, which alters their adsorption properties as evidenced by CO-DRIFTS.[13] The lower specific surface area and smaller characteristic pore size of the commercial θ–α-Al_2O_3 support are expected to only have minor influence on the catalyst performance during low-temperature dehydrogenation. While both can lower the surface concentration of active sites and increase susceptibility to internal mass transfer limitations in liquid-filled pores,[17,33,44] transport effects are not expected to dominate in tested powder catalysts.[56]

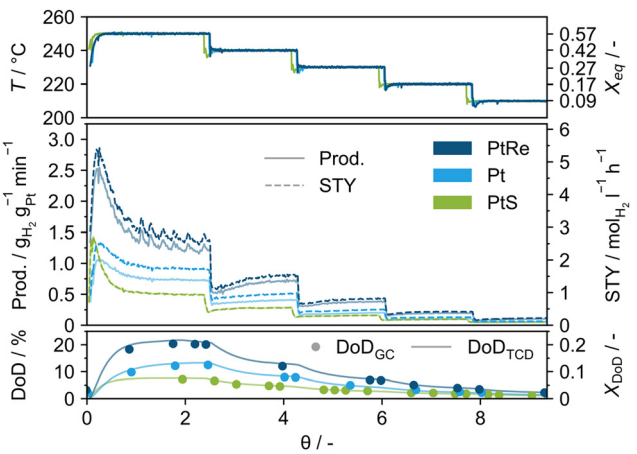

Fig. 3 Effect of temperature on key performance indicators of PtRe, Pt and PtS catalyst for continuous dehydrogenation of perhydro benzyltoluene (H12-BT) at 1000 rpm, 1 bar_a, and a H12-BT feed rate of 2.0 ml min^{-1}. PtS data adapted from previous work.[55] The data illustrate the temperature sensitivity of the reactor and catalyst systems under continuous slurry operation in the studied temperature range (210–250 °C).

Conclusively, the catalysts exhibit stable and reproducible performance under continuous operation, which enables ranking based on the steady-state activity. Across the investigated temperature range, PtRe consistently shows the highest activity, followed by Pt and PtS.

3.3. Reactor dependent performance and scaling behaviour

A direct comparison of the absolute hydrogen productivity measured in the CSTR and during semi-batch testing at comparable DoDs (Fig. S9) reveals a systematic difference between both reactor concepts across the investigated temperature range (Fig. 4, Table S7). For all catalysts and temperatures, semi-batch operation results in substantially higher productivity exceeding the corresponding CSTR values by a factor of three to five. This indicates that semi-batch screening consistently overestimates the achievable productivity under steady-state conditions.

Despite the systematic offset of absolute productivity, the order of catalyst activity remains largely unchanged. When productivity is normalised to the most active catalyst at each temperature (Fig. 4), similar trends are apparent in both

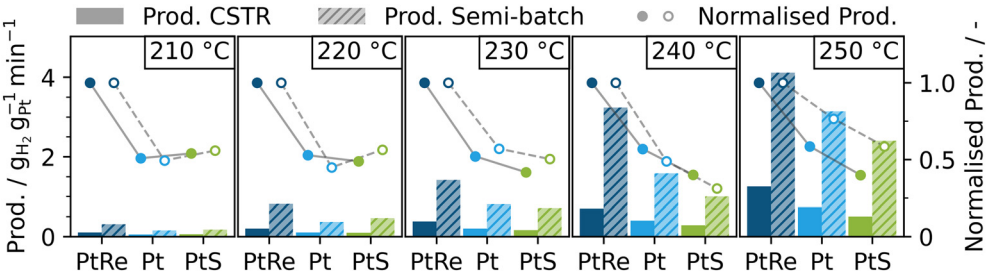

Fig. 4 Productivity measured during continuous stirred-tank reactor (CSTR) and semi-batch operation for PtRe, Pt, and PtS catalysts at reaction temperatures between 210 and 250 °C. CSTR PtS data adapted from previous work.[55] Semi-batch data for PtRe and Pt adapted from Strauch *et al.*[48] All productivity values are reported at comparable degrees of dehydrogenation (DoD). Solid bars represent productivity obtained in the CSTR at steady-state, while patterned bars indicate semi-batch data. Symbols denote productivity values normalised to the most active catalyst at each temperature level with lines to guide the eye.

semi-batch and continuous operation. However, minor deviations are evident, particularly for Pt and PtS at lower temperatures. These observations suggest that, while semi-batch screening reliably identifies the most active catalyst and captures overall performance trends, it does not quantitatively reproduce absolute productivity levels and can partially distort the relative spacing between catalysts under continuous conditions.

To evaluate whether the difference between semi-batch and continuous operation follows a systematic, reactor dependent trend, the temperature dependence of hydrogen productivity was analysed on a logarithmic scale for both reactor concepts (Fig. 5(a)). For all catalysts, productivity increases exponentially with temperature in both systems, resulting in roughly parallel trends when plotted against temperature. Although the fitted trends for both reactor concepts capture the overall temperature dependence, the scatter of the individual semi-batch data points around the fitted lines is slightly larger than during continuous testing. This reflects the fact that the semi-batch data was obtained from independent transient experiments, whereas the CSTR data represent steady-state operation during a single experiment with mean productivity values acquired during several residence times. Notably, this increased scatter does not affect the observed systematic offset.

Further inspection of the logarithmic productivity data reveals a consistent difference between CSTR and semi-batch operation across catalysts and temperatures (Table S7). The difference between the log-transformed CSTR and semi-batch productivities remains narrow within $\Delta\log(\text{Prod.}) \approx 0.5$–$0.7$ for PtRe, Pt, and PtS throughout the investigated temperature window. The similarity of the slopes on a logarithmic scale and the lack of strong temperature dependence in $\Delta\log(\text{Prod.})$ indicate that the underlying temperature sensitivity is largely preserved, while the absolute rate level is shifted by the reactor configuration. In this sense, the productivity difference may, as a first approximation, be described by a common reactor dependent scaling factor.

Across the investigated temperature range, the ratio between the absolute productivities remains within a relatively narrow range and only shows a minor temperature dependence (Fig. 5(b), Table S7). The absence of a pronounced monotonic trend further supports the interpretation that the lower productivity observed in continuous operation reflects a systematic reactor dependent

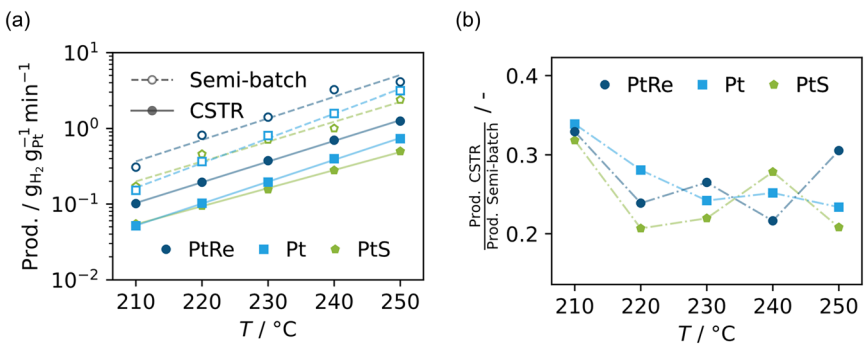

Fig. 5 (a) Temperature dependence of the productivity, as measured during continuous stirred-tank reactor (CSTR) and semi-batch operation for PtRe, Pt and PtS catalysts at comparable degrees of dehydrogenation (DoD). Productivity is shown on a logarithmic scale with linear fit to illustrate the systematic offset between the two reactor types. (b) Ratio of CSTR to semi-batch productivity, as function of temperature for the three catalysts. This highlights the approx. constant, reactor dependent scaling behaviour across the investigated temperature range, although the 210 °C data points show comparatively high values for all catalysts. Lines to guide the eye. CSTR PtS data adapted from previous work.[55] Semi-batch data for PtRe and Pt adapted from Strauch *et al.*[48]

shift that can be approximated by a common scaling factor, rather than isolated operating effects.

3.4. Transferability between reactor concepts

The systematic productivity offset identified in the logarithmic and ratio analyses suggests that semi-batch data can be transferred to continuous operation at a qualitative, but not quantitative, level. To further assess transferability between reactor concepts, CSTR and semi-batch productivity values at comparable DoD were related by the empirical transfer expression given in eqn (12), introducing an effective transfer factor φ.

$$\varphi = \left.\frac{\text{Prod. CSTR}}{\text{Prod. Semi-batch}}\right|_{\text{DoD},T,p,\text{LOHC:Pt}} \quad (12)$$

In the case of ideal quantitative transferability between reactor concepts, φ = 1 would be expected. However, correlating CSTR and semi-batch productivity values in a parity plot reveals systematic deviations from one-to-one correspondence (Fig. 6). Origin-constrained fits require effective transfer factors of 0.27 for PtRe, 0.24 for Pt, and 0.22 for PtS. Therefore, only 20–30% of semi-batch productivity is observed during continuous operation. Notably, the magnitude of φ depends on the catalyst, with the largest value obtained for PtRe, the most active catalyst in both reactor systems. This indicates that higher catalyst activity is associated not only with higher absolute productivity, but also with somewhat improved quantitative transferability between semi-batch and continuous operation. At the same time, the transfer factors remain within a comparatively narrow range, corresponding to an average value of $\varphi \approx 0.24$ for the investigated system. This suggests that a reactor dependent empirical transfer factor can serve as a useful first approximation, or rule-of-thumb, for estimating continuous CSTR productivity from semi-batch data. However, φ-scaled parity analysis (Fig. S10) demonstrates that this scaling does not fully collapse all data onto parity, indicating residual temperature and catalyst dependent deviations. Consequently, semi-batch screening captures catalyst ranking and general performance trends reliably, whereas quantitative transferability to continuous operation remains reactor and catalyst dependent and improves with increasing activity.

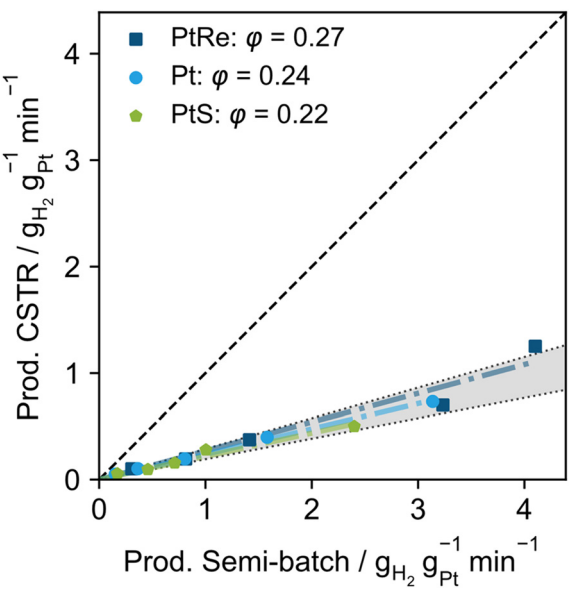

Fig. 6 Parity plot of productivity during continuous (CSTR) and semi-batch dehydrogenation conditions for PtRe, Pt, and PtS catalysts at comparable degrees of dehydrogenation (DoD). Dash-dotted lines represent origin-constrained linear fits, $y = \varphi x$, for the individual catalysts. Dotted lines and shaded region indicate a ±20% deviation envelope around the average empirical transfer relationship, $y = 0.24x$, which corresponds to the mean effective transfer factor of the investigated system and is included as a visual guide only and not as a statistically derived confidence interval. Effective transfer factors below unity indicate a systematic underestimation of the productivity during continuous operation relative to semi-batch, while the preserved correlation reflects qualitative transferability of catalyst performance trends between reactor concepts. CSTR PtS data adapted from previous work.[55] Semi-batch data for PtRe and Pt adapted from Strauch *et al.*[48]

The systematic offset between CSTR and semi-batch productivity can be explained by a range of parameters affecting the reactor environment. Firstly, semi-batch experiments follow a transient composition trajectory and therefore include an initially favourable high-rate regime similar to the elevated productivity observed during start-up in continuous operation (Fig. 3), which is also 2–3 times higher than during steady-state. At steady-state, the productivity in a CSTR is consequently lower due to a lower driving force for dehydrogenation, which results in systematic underestimation of the productivity during continuous operation. Additional contributions may arise from potential differences in local hydrogen partial pressure, catalyst deposition on the reactor internals observed after reaction, mixing intensity, catalyst suspension, and agitation mode. In particular, magnetic stirring was used in the semi-batch setup, whereas the continuous CSTR was mechanically stirred, which may influence solid–liquid contact, and hydrogen removal. Related LOHC studies likewise show that hydrogen release strongly depends on reactor concept and local reaction environment, including hydrogen removal from the reactor, pressure level, and system design.[54,64–67] Notably, Mahayni *et al.*[38] reported comparable H12-BT dehydrogenation productivity in semi-batch operation and continuous fixed-bed validation for Pt/Al_2O_3 catalysts with optimised Pt nanoparticle size. However, this comparison was performed in a fixed-bed reactor using shaped catalyst pellets rather than in a single CSTR, and therefore reflects transferability to a different continuous reactor concept. This distinction highlights that reactor-to-reactor transfer is not governed by the operation mode alone, but also by the specific hydrodynamic and transport environment. These findings support the interpretation that the systematic offset

observed here originates from reactor specific transport, mixing, and pressure effects. However, in the LOHC literature considered here, these effects are discussed in a reactor specific manner and do not provide a direct mapping between semi-batch data and continuous performance. The broader reaction engineering literature has addressed the transferability from semi-batch to continuous reactor concepts more explicitly, although direct experimental comparisons between semi-batch and single-CSTR remain limited. Florit *et al.*[68] developed kinetics-free procedures for transforming semi-batch recipes to equivalent continuous tubular reactors or CSTR cascades with intermediate feeding, and Maestri *et al.*[69] extended this concept into a general experimental procedure for fine chemicals. Copelli *et al.*[70] applied this framework to potentially runaway nitration, demonstrating that a CSTR cascade could replicate the semi-batch process with a significantly smaller reactor volume while ensuring safe operation. More generally, comparative studies on other reaction systems have shown that changing from semi-batch to continuous operation can affect the observed conversion, selectivity, productivity or product quality, since the dosing strategy, residence time, mixing and transport conditions differ between reactor concepts.[71–74] The present results are consistent with this broader picture while extending it to H12-BT dehydrogenation under experimentally matched conditions.

3.5. Apparent kinetics and temperature dependence

All catalyst tests were conducted significantly below equilibrium conversion (Fig. 3), which enables analysis of the apparent reaction kinetics. Arrhenius-type analyses were therefore performed to assess whether the observed differences between CSTR and semi-batch operation are mainly reflected in the apparent rate level or also in the temperature sensitivity (Fig. 7). For all catalysts, linear relationships are obtained, which is consistent with a predominantly kinetic temperature dependence, *i.e.* operation in the kinetic regime.[75]

Several considerations indicate that the derived Arrhenius parameters are unlikely to be primarily governed by non-kinetic limitations under the investigated conditions. First, the temperature range of 210–250 °C is below the elevated-temperature regime in which significant mass or heat transfer limitations during H12-BT dehydrogenation have mainly been reported.[56,76] Second, previous investigations using the same three-phase slurry CSTR concept, LOHC system, PtS catalyst, and catalyst particle size range showed that catalyst productivity became largely independent of stirrer speed once complete catalyst suspension was achieved.[55] This indicates that mixing-sensitive external transport was not rate-dominant under the selected conditions. Gas–liquid transport requires separate consideration because hydrogen is a reaction product and its transfer into the liquid phase does not limit reactant supply. Although bubble-nucleation limitations can occur, vigorous stirring has been demonstrated as mitigation strategy.[14] Hence, their influence is expected to be small, although effects on gas holdup, local hydrogen partial pressure, and disengagement cannot be excluded. Third, a particle size study for H12-BT dehydrogenation using the same commercial PtS catalyst found pore-diffusion effects for the original shaped catalyst bodies, but no further rate increase for particles below 500 μm.[56] Since the particle fractions used in this work were below this threshold, dominant intraparticle diffusion is considered unlikely, although minor contributions cannot be excluded. Finally, no systematic loss of activity was observed during continuous operation. For the commercial PtS catalyst, stable activity was additionally demonstrated during long-term operation at 310 °C,[55] indicating that catalyst deactivation is not dominant within the investigated operating range.

The apparent activation energies across operation modes (Table 3) are within the typical error margin for each catalyst. This indicates that the temperature sensitivity of the dehydrogenation reaction remains largely unchanged. Consequently, the corresponding pre-exponential factors (Table 3) reflect shifts in the apparent rate level under the respective reactor configuration. This observation supports the conclusion that reactor dependent effects primarily influence the rate magnitude while catalyst specific trends in temperature sensitivity remain intact. The derived Arrhenius parameters therefore represent apparent kinetic descriptors that integrate

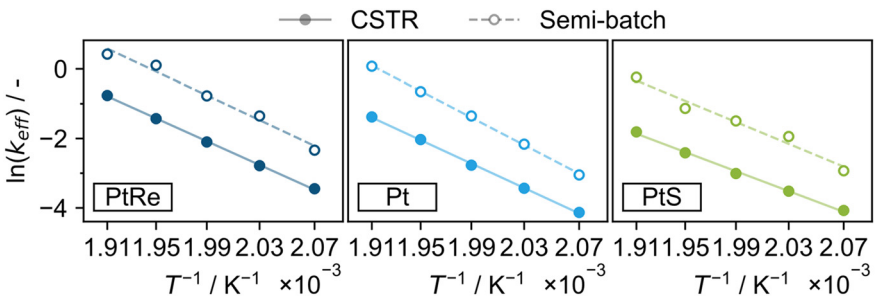

Fig. 7 Arrhenius plots for continuous (CSTR) and semi-batch dehydrogenation over PtRe, Pt and PtS catalysts. Lines represent the linear regression used to determine the Arrhenius parameters. The data quantify the temperature sensitivity of the tested catalysts in the studied temperature range (210–250 °C). CSTR PtS adapted from previous work.[55] Semi-batch data for PtRe and Pt adapted from Strauch *et al.*[48]

Table 3 Apparent activation energies $E_{A,e}$ and pre-exponential factors k_0 derived from Arrhenius analyses of perhydro benzyltoluene dehydrogenation over PtRe, Pt and PtS catalysts under continuous (CSTR) and semi-batch operation. PtRe and Pt, semi-batch values reported by Strauch *et al.*[48] were re-evaluated using the same normalisation approach applied to the CSTR data to ensure methodological consistency

Catalyst	$E_{A,e}$/kJ mol^{-1}	k_0/l$_{Hx\text{-}BT}$ kg$_{Pt}^{-1}$ s^{-1}	Setup	Ref.
PtRe	141	5.86×10^{13}	CSTR	This study
	147[a]	8.47×10^{14}	Semi-batch	48
Pt	145	7.79×10^{13}	CSTR	This study
	163[a]	2.91×10^{16}	Semi-batch	48
PtS	118	1.02×10^{11}	CSTR	55
	130	7.08×10^{12}	Semi-batch	This study

[a] Apparent activation energies differ from reported values due the use of a modified kinetic approach with the concentration of hydrogenated BT equivalents $c_{Hx\text{-}BT}$, see eqn (10), as well as extraction of the productivity in the DoD range of corresponding CSTR experiments.

intrinsic reaction kinetics with reactor specific transport, hydrodynamic, and compositional effects.

Systematically derived Arrhenius parameters for perhydro benzyltoluene dehydrogenation are scarce in the open literature and are strongly affected by the testing environment as well as data evaluation. Jo *et al.*[17] report apparent activation energies of 168 kJ mol^{-1} for a mesoporous platinum on alumina catalyst (2.67 wt% Pt) and 111 kJ mol^{-1} for a sulphur modified catalyst (2.70 wt% Pt, 0.21 wt% S) during semi-batch testing. This is consistent with the trend observed in the present study, where the sulphur-modified Pt catalyst exhibits lower apparent activation energies than the unmodified Pt catalyst, regardless of the operation mode.

Strauch *et al.*[48] report apparent activation energies of 170.5 and 182.2 kJ mol^{-1} for PtRe and Pt, respectively, when comparing the maximum productivity at low DoD (DoD ≈ 5%) during semi-batch operation. At such a low DoD, changes in liquid phase composition as well as inhibition and coverage effects are neglectable. To reduce the influence of conversion level on the kinetic analysis during continuous operation, the effective formation rate of hydrogen was herein normalised to the concentration of hydrogenated BT equivalents, $c_{Hx\text{-}BT}$ (eqn (10)), thereby accounting for the decreasing concentration of hydrogenated carrier with increasing DoD. While this normalisation takes the conversion level into account, it cannot eliminate effects entirely as changes in liquid phase composition (distribution of partially dehydrogenated intermediates) and the associated adsorption or inhibition phenomena cannot be captured by a single concentration term. Applying this evaluation approach to the semi-batch productivity data reported by Strauch *et al.*,[48] apparent activation energies of 147 and 163 kJ mol^{-1} were obtained for PtRe and Pt, respectively (Table 3). The lower values can mostly be attributed to higher DoD levels at higher temperatures, where the effects of inhibition or coverage are more pronounced and affect the effective Arrhenius parameters.

While the Arrhenius analysis quantifies the transferability of temperature dependence and the reactor dependent shift in the apparent rate level, this behaviour is illustrated directly by plotting the effective rate constant for the studied temperature range (Fig. 8). Derived from the Arrhenius parameters (Table 3), the plot shows that k_{eff} increases monotonically with temperature for both reactor concepts, with semi-batch operation consistently yielding higher rate constants than continuous operation. Although the offset between the two reactor concepts remains relatively constant, the difference in their effective rate constants scales with temperature. This trend reflects differences in the pre-exponential factors and confirms that the effects of the reactor primarily manifest as shifts in the reaction rate rather than the temperature sensitivity.

3.6. Liquid phase analysis and side reactions

Liquid phase analysis was conducted to investigate whether the reactor configuration influences the reaction pathway or

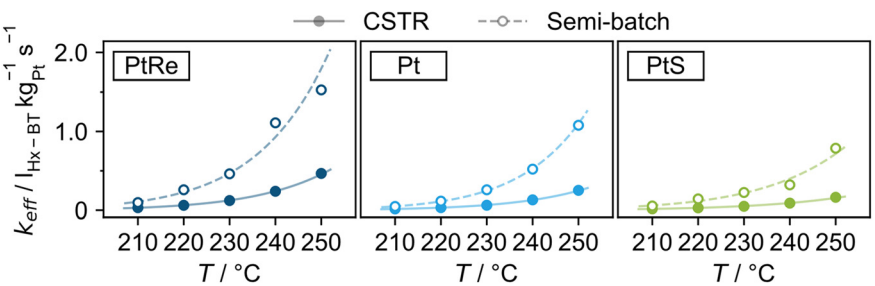

Fig. 8 Temperature dependence of the effective rate constant k_{eff} for continuous (CSTR) and semi-batch dehydrogenation over PtRe, Pt and PtS catalysts. Lines are calculated from previously determined $E_{A,e}$ and k_0 (eqn (11)) and illustrate reactor dependent differences in the effective rate level. CSTR PtS data adapted from previous work.[55] Semi-batch data for PtRe and Pt adapted from Strauch *et al.*[48]

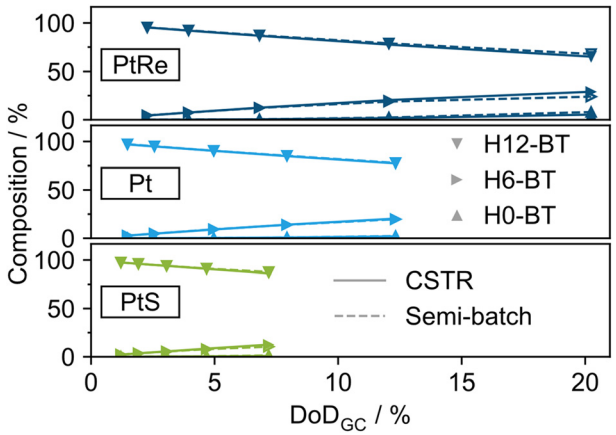

Fig. 9 Liquid phase composition at various degrees of dehydrogenation (DoD$_{GC}$) for continuous (CSTR) and semi-batch dehydrogenation over PtRe, Pt and PtS catalysts. The relative fractions of H12-BT, H6-BT and H0-BT are shown. Similar product distributions at comparable DoD suggest a reactor independent reaction pathway, whereas small differences suggest a mild separation by boiling point within the CSTR. Lines to guide the eye. CSTR PtS adapted from previous work.[55] Semi-batch data for PtRe and Pt adapted from Strauch *et al.*[48]

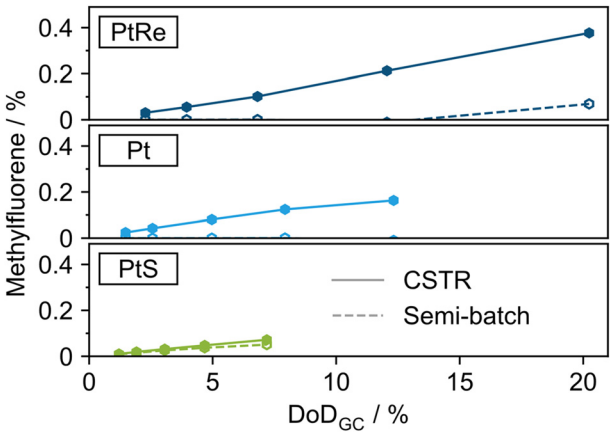

Fig. 10 Formation of methylfluorene at various degrees of dehydrogenation (DoD$_{GC}$) for continuous (CSTR) and semi-batch dehydrogenation over PtRe, Pt and PtS catalysts. Continuous operation results in higher concentrations of methylfluorene at comparable DoD$_{GC}$, with this effect being most pronounced for the highly active PtRe catalyst. These trends suggest that side-product formation is enhanced under conditions where partially dehydrogenated intermediates remain in the reactor for longer, emphasising the reactor dependent aspect of consecutive reactions. Lines to guide the eye. CSTR PtS data adapted from previous work.[55] Semi-batch data for PtRe and Pt adapted from Strauch *et al.*[48]

primarily affects the liquid phase composition through operation mode (Fig. 9). When product composition is compared at similar DoD, the overall composition follows the same qualitative trends for both CSTR and semi-batch operation. This suggests that the primary dehydrogenation sequence remains consistent in both operation modes. However, differences in intermediate holdup and phase behaviour specific to each reactor slightly modify the liquid phase composition and the extent of consecutive side reactions. In particular, CSTR operation results in a slightly lower H12-BT fraction and more pronounced accumulation of H6-BT at comparable DoD, most notably for the highly active PtRe catalyst. While this trend also reflects comparison of steady-state with transient composition, it may also be linked to a preferential evaporation of the BT species with a lower boiling point and a discharge *via* the gas phase in the CSTR.[55] These BT species are refluxed during semi-batch operation. The more pronounced shift in composition observed for PtRe can be explained by its higher hydrogen production rate and the resulting increased gas flow out of the reactor increasing discharge of evaporated perhydro benzyltoluene.[54] These effects modify the liquid phase composition without altering the underlying reaction sequence and therefore reflect physical separation by the CSTR.

The DoD observed under steady-state CSTR operation is reached in semi-batch experiments after approx. 20–30 min (Fig. S11). The reproducible timescale observed across experiments indicates that CSTR operation stabilises the system at an early point along the dehydrogenation pathway. Notably, this characteristic semi-batch timescale is substantially shorter than the mean residence time of the CSTR (approx. 135 min under standard conditions). Increasing the residence time shifts the steady-state of the CSTR towards later times in semi-batch operation (Fig. S12). This behaviour is originated in the strongly mixed nature of the CSTR and the continuous replenishment of fresh H12-BT and withdrawal of partially dehydrogenated liquid, as well as the sequential, equilibrium limited nature of the dehydrogenation network. Consequently, the continuous reactor stabilises at an intermediate H6-BT-rich composition and does not access the deeper conversion regime explored during longer semi-batch operations.

Side product formation is a critical aspect of LOHC dehydrogenation as Pt-based catalysts also accelerate deep dehydrogenation of H0-BT and other consecutive reactions, such as cyclisation, leading to methylfluorene and other high boiling by-products.[7,19,21] These reactions lower selectivity towards H0-BT as well as the LOHC quality and consequently may affect the hydrogen capacity over repeated storage cycles. The formation of methylfluorene increases systematically with the degree of dehydrogenation for all the catalysts (Fig. 10). At a comparable DoD, CSTR operation results in higher methylfluorene concentrations than semi-batch operation, with this effect being most pronounced for the highly active PtRe catalyst. As methylfluorene is formed *via* consecutive reaction of most likely H6-BT and H0-BT, the prolonged residence time in the reactor promotes the formation of side products. Hence, the side product formation scales with exposure time of the catalyst to (partially) dehydrogenated species. Further, the absolute turnovers of H6-BT are seemingly more important than the actual exposure of H0-BT to the catalyst, *i.e.* the data comparison suggests that methylfluorene species rather form

via consecutive dehydrogenation rather than through re-adsorption of H0-BT. In contrast, PtS consistently showed the lowest methylfluorene concentrations among the investigated catalysts, indicating a reduced tendency towards consecutive side reactions. This is in line with the concept of sulphur modification of PtS, where selective poisoning preserves the dehydrogenation activity of platinum while suppressing hydrogenolysis and by-product formation, thereby improving catalyst stability.[13,77] The general observed trends suggest methylfluorene formation in the CSTR reflects residence time and accumulation effects dependent on the reactor rather than a change in the underlying reaction pathway. These findings further support the conclusion that the differences between semi-batch and continuous reactor concepts arise from the operational realisation of the same reaction network, rather than changes in catalyst selectivity or reaction mechanisms.

4. Summary and conclusions

A systematic comparison of CSTR and semi-batch operation for the dehydrogenation of perhydro benzyltoluene over PtRe, Pt and PtS catalysts revealed that semi-batch screening does reliably represent the qualitative catalyst performance. However, a systematic overprediction of the steady-state productivity in continuous operation was identified rendering quantitative transfer of semi-batch results to continuous operation challenging. Across the investigated temperature range (210–250 °C), semi-batch productivities were approx. three to five times higher than the corresponding CSTR values at steady-state, while the catalyst order remained unchanged at PtRe > Pt > PtS. Noteworthy, the transient productivity during start-up of the CSTR is only 2–3 times increased, *i.e.* continuous operation is already reflected in the early time on stream.

The difference between the two reactor concepts was shown to be systematic and reactor dependent. Logarithmic, ratio, and parity analyses revealed that this difference can be approximated by a reactor specific empirical transfer factor. However, the extent of quantitative transferability remains in part catalyst specific as the effect of catalyst performance on the liquid composition remains relevant. Apparent kinetic analysis revealed similar temperature sensitivities in both reactor types, whereas liquid phase analysis showed that they both follow the same primary dehydrogenation pathway. Therefore, the lower continuous productivity is not attributed to a change in the underlying chemistry, but to the different reactor environments sampled by CSTR and semi-batch operation. Continuous stirred operation stabilises the system at an earlier, H6-BT-rich position along the dehydrogenation network.

These findings demonstrate that semi-batch testing represents an effective tool for catalyst screening and benchmarking. However, quantitative reactor and process assessment for LOHC hydrogen release requires validation under the relevant continuous operating mode. In this sense, the present study provides a framework for relating semi-batch screening results to steady-state CSTR performance, yielding valuable insight into the general relationship between transient screening data and continuous LOHC dehydrogenation.

Author contributions

Elisabeth Herzinger: writing – review & editing, writing – original draft, visualization, validation, methodology, investigation, formal analysis, data curation, conceptualization. Jona Berger: investigation, formal analysis. Nicolas Patrick Johner: writing – review & editing, investigation, formal analysis. Franziska Auer: writing – review & editing, supervision, resources, project administration. Moritz Wolf: writing – review & editing, validation, supervision, resources, project administration, methodology, funding acquisition, conceptualization.

Conflicts of interest

There are no conflicts to declare.

Symbols

$c_{A,0}$	Initial concentration of component *A* (mol l^{-1})
c_A	Liquid phase concentration of component *A* (mol l^{-1})
$c_{A,end}$	Concentration of component *A* at the end of the experiment (mol l^{-1})
$c_{A,SS}$	Concentration of component *A* at steady-state (mol l^{-1})
$c_{H12\text{-}BT}$	Concentration of H12-BT (mol l^{-1})
$c_{Hx\text{-}BT}$	Concentration of hydrogenated BT equivalents (mol l^{-1})
d_{BJH}	Average pore diameter (nm)
DoD	Degree of dehydrogenation (%)
DoD_{GC}	Degree of dehydrogenation according to GC-FID (%)
DoD_{TCD}	Degree of dehydrogenation according to TCD (%)
DoH	Degree of hydrogenation (%)
$DoH_{eq,BT}$	Equilibrium degree of hydrogenation (—)
D_{Pt}	Apparent platinum dispersion (%)
ΔProd.	Relative change in productivity (%)
Δt	Time interval (min)
$E_{A,e}$	Arrhenius activation energy (kJ mol^{-1})
k_0	Pre-exponential factor ($l_{Hx\text{-}BT}$ kg_{Pt}^{-1} s^{-1})
k_{eff}	Effective reaction rate constant ($l_{Hx\text{-}BT}$ kg_{Pt}^{-1} s^{-1})
m_{cat}	Catalyst mass (g)
m_{H_2}	Mass of released hydrogen (g)
M_{H_2}	Molar mass of hydrogen (g mol^{-1})
m_{Pt}	Mass of platinum (g)
M_{Pt}	Molar mass of platinum (g mol^{-1})
$\dot{n}$	Molar flow of formed product (mol h^{-1})

$\dot{n}_{H_2}$	Molar flow of formed hydrogen (mol s^{-1})
n_{eff}	Effective reaction order (—)
n_{Pt}	Molar amount of platinum (mol)
pH_{PZC}	pH at the point of zero charge (—)
Prod.	Platinum-based productivity (g_{H_2} g_{Pt}^{-1} min^{-1})
φ	Effective transfer factor from semi-batch to continuous operation (—)
R	Universal gas constant (J mol^{-1} K^{-1})
$r_{H_2,eff}$	Effective formation rate of hydrogen (mol_{H_2} kg_{Pt}^{-1} s^{-1})
ρ_{H_2}	Density of hydrogen (kg m^{-3})
S_{BET}	Specific surface area (m^2 g^{-1})
STY	Space–time yield (mol_{H_2} l^{-1} h^{-1})
t	Time (min)
t_{end}	Reaction time at end of experiment (min)
T	Temperature (K)
τ	Residence time (min)
θ	Dimensionless time (—)
TOF	Turnover frequency (s^{-1})
V	Volume (ml)
$\dot{V}_{H12\text{-}BT}$	Volumetric H12-BT flow rate (ml min^{-1})
$\dot{V}_{H_2}$	Volumetric hydrogen flow rate (ml min^{-1})
V_m	Molar gas volume under standard conditions (l mol^{-1})
V_R	Reaction Volume (ml)
w_{Pt}	Platinum loading (wt%)
X	Conversion (—)
X_{eq}	Equilibrium conversion (—)
X_{DoD}	conversion of dehydrogenation (—)
x_{Fl}	Mole fraction of methylfluorene (—)
$x_{H0\text{-}BT}$	Mole fraction of H0-BT (—)
$x_{H12\text{-}BT}$	Mole fraction of H12-BT (—)
$x_{H6\text{-}BT}$	Mole fraction of H6-BT (—)
x	Position in the reactor (—)

Data availability

All data is openly available on Repo4Cat (https://repository.nfdi4cat.org/) *via* the link: https://hdl.handle.net/21.11165/4cat/6rb2-s364.

Supplementary information (SI) is available. See DOI: https://doi.org/10.1039/d6re00193a.

Acknowledgements

Financial support by the Helmholtz Research Program "Materials and Technologies for the Energy Transition (MTET), Topic 3: Chemical Energy Carriers", and the Strategy Funds of the KIT Executive Board are highly acknowledged. Clariant and Hydrogenious LOHC Technologies are thanked for providing the commercial catalyst EleMax D, while Hydrogenious LOHC Technologies is also acknowledged for the provision of perhydro benzyltoluene. Dr. Domenic Strauch is thanked for providing additional liquid phase data beyond the values reported in the published work. Appreciation is extended to Dr. Timo Schaerfe (né Rüde) for his insights into liquid sample analysis and for providing the code used to evaluate the data. Input on data management for the three-phase slurry reactor and the evaluation of kinetic parameters by Jakob Biesinger is highly acknowledged. Dr. Thomas Zevaco and Ozan Kırlangıçoğlu are thanked for the high-quality, publication-ready photographs. The glassblowing and mechanical workshops are gratefully acknowledged for their support in manufacturing custom components and implementing modifications to the reactor setups. Armin Lautenbach determined the metal content by inductively coupled plasma atomic emission spectrometry and Dr. Thomas Otto provided the N_2 physisorption isotherms. Microsoft Copilot and DeepL Write were used to assist with phrasing and language refinement, followed by careful review and editing by the authors.

References

1 E. Herzinger and M. Wolf, Perspectives and Potential of Liquid Organic Hydrogen Carriers in the German Energy Scenario, *Chem. Ing. Tech.*, 2024, **96**, 65–73.
2 P. Preuster, C. Papp and P. Wasserscheid, Liquid Organic Hydrogen Carriers (LOHCs): Toward a Hydrogen-free Hydrogen Economy, *Acc. Chem. Res.*, 2017, **50**, 74–85.
3 P. C. Rao and M. Yoon, Potential Liquid-Organic Hydrogen Carrier (LOHC) Systems: A Review on Recent Progress, *Energies*, 2020, **13**, 6040.
4 Z. Cai, C. Zou, X. Jiang, L. Liu, Y. Chen, W. Zhuang, I. Shakir, H. Peng, W. Hu, X. Sun and Y. Yao, Toward a green hydrogen economy: progress, economic feasibility, and challenges of liquid organic hydrogen carriers, *Green Chem.*, 2025, **27**, 12856–12887.
5 S. O. Akpasi, I. M. Smarte Anekwe, E. K. Tetteh, U. O. Amune, S. I. Mustapha and S. L. Kiambi, Hydrogen as a clean energy carrier: advancements, challenges, and its role in a sustainable energy future, *Clean Energy*, 2025, **9**, 52–88.
6 M. A. Sattar, M. G. Rasul, M. I. Jahirul and M. M. Hasan, An up-to-date review on the progress and challenges of hydrogen storage, and its safety and economic analysis, *Sustainable Energy Fuels*, 2024, **8**, 3545–3573.
7 T. Rüde, S. Dürr, P. Preuster, M. Wolf and P. Wasserscheid, Benzyltoluene/perhydro benzyltoluene – pushing the performance limits of pure hydrocarbon liquid organic hydrogen carrier (LOHC) systems, *Sustainable Energy Fuels*, 2022, **6**, 1541–1553.
8 N. Brückner, K. Obesser, A. Bösmann, D. Teichmann, W. Arlt, J. Dungs and P. Wasserscheid, Evaluation of industrially applied heat-transfer fluids as liquid organic hydrogen carrier systems, *ChemSusChem*, 2014, **7**, 229–235.
9 G. Cabrera, M. Mora, J. P. Gil-Burgos, R. Visbal, F. Machuca-Martínez and E. Mosquera-Vargas, Liquid Organic Hydrogen Carrier Concepts and Catalysts for Hydrogenation and Dehydrogenation Reactions, *Molecules*, 2024, **29**, 4938.
10 Y. Jo, J. Oh, D. Kim, J. H. Park, J. H. Baik and Y.-W. Suh, Recent progress in dehydrogenation catalysts for

heterocyclic and homocyclic liquid organic hydrogen carriers, *Korean J. Chem. Eng.*, 2022, **39**, 20–37.
11 R. Tan, Q. Ji, Y. Ling and L. Li, Advances in liquid organic hydrogen carriers: developing efficient dehydrogenation strategies, *Chem. Commun.*, 2024, **60**, 8186–8203.
12 J. Ba, R. Gao, D. Shi, H. A. Nessa, C. Shi, X. Zhang, L. Pan and J.-J. Zou, Progress in catalysts for hydrogen storage/release in MBT/DBT based LOHCs: a review, *Chem. Commun.*, 2025, **61**, 8619–8631.
13 F. Auer, D. Blaumeiser, T. Bauer, A. Bösmann, N. Szesni, J. Libuda and P. Wasserscheid, Boosting the activity of hydrogen release from liquid organic hydrogen carrier systems by sulfur-additives to Pt on alumina catalysts, *Catal. Sci. Technol.*, 2019, **9**, 3537–3547.
14 T. Solymosi, M. Geißelbrecht, S. Mayer, M. Auer, P. Leicht, M. Terlinden, P. Malgaretti, A. Bösmann, P. Preuster, J. Harting, M. Thommes, N. Vogel and P. Wasserscheid, Nucleation as a rate-determining step in catalytic gas generation reactions from liquid phase systems, *Sci. Adv.*, 2022, **8**, eade3262.
15 E.-R. On, K. Lee, Y. Kwak, C. Kim, Q. Dao, H. Sohn, S. W. Nam, J. Kim, Y. Kim and H. Jeong, Promoter-Guided Reaction Intermediate Dynamics Enhance Perhydro-benzyltoluene Dehydrogenation, *ACS Catal.*, 2025, **15**, 5531–5545.
16 X. Chen, C. H. Gierlich, S. Schötz, D. Blaumeiser, T. Bauer, J. Libuda and R. Palkovits, Hydrogen Production Based on Liquid Organic Hydrogen Carriers through Sulfur Doped Platinum Catalysts Supported on TiO_2, *ACS Sustainable Chem. Eng.*, 2021, **9**, 6561–6573.
17 Y. Jo, T. W. Kim, J. Oh, D. Kim and Y.-W. Suh, Mesoporous sulfur-decorated Pt–Al_2O_3 for dehydrogenation of perhydro benzyltoluenes: Activity-favorable adsorption of reaction species onto electron-deficient Pt atoms, *J. Catal.*, 2022, **413**, 127–137.
18 F. Auer, A. Hupfer, A. Bösmann, N. Szesni and P. Wasserscheid, Influence of the nanoparticle size on hydrogen release and side product formation in liquid organic hydrogen carrier systems with supported platinum catalysts, *Catal. Sci. Technol.*, 2020, **10**, 6669–6678.
19 K. Alconada, F. Mariño, I. Agirre and V. L. Barrio, Exploring Perhydro-Benzyltoluene Dehydrogenation Using Sulfur-Doped PtMo/Al_2O_3 Catalysts, *Catalysts*, 2025, **15**, 485.
20 N. Marchenko, M. Kharma, L. Pinard, L. Massin, F. Morfin, L. Piccolo, N. Batalha and V. Meille, Effect of titania phase on the performance of Pt/TiO_2 catalysts in the dehydrogenation of perhydrobenzyltoluene, *Int. J. Hydrogen Energy*, 2025, **161**, 150636.
21 B. Bong, C. Mebrahtu, D. Jurado, A. Bösmann, P. Wasserscheid and R. Palkovits, Hydrogen Loading and Release Potential of the LOHC System Benzyltoluene/Perhydro Benzyltoluene over S–Pt/TiO_2 Catalyst, *ACS Eng. Au*, 2024, **4**, 359–367.
22 P. T. Aakko-Saksa, M. Vehkamäki, M. Kemell, L. Keskiväli, P. Simell, M. Reinikainen, U. Tapper and T. Repo, Hydrogen release from liquid organic hydrogen carriers catalysed by platinum on rutile-anatase structured titania, *Chem. Commun.*, 2020, **56**, 1657–1660.
23 S. Lee, J. Lee, T. Kim, G. Han, J. Lee, K. Lee and J. Bae, Pt/CeO_2 catalyst synthesized by combustion method for dehydrogenation of perhydro-dibenzyltoluene as liquid organic hydrogen carrier: Effect of pore size and metal dispersion, *Int. J. Hydrogen Energy*, 2021, **46**, 5520–5529.
24 C.-I. Ahn, Y. Kwak, A.-R. Kim, M. Jang, A. Badakhsh, J. Cha, Y. Kim, Y. S. Jo, H. Jeong, S. H. Choi, S. W. Nam, C. W. Yoon and H. Sohn, Dehydrogenation of homocyclic liquid organic hydrogen carriers (LOHCs) over Pt supported on an ordered pore structure of 3-D cubic mesoporous KIT-6 silica, *Appl. Catal., B*, 2022, **307**, 121169.
25 H.-L. Ye, S.-X. Liu, C. Zhang, Y.-Q. Cai and Y.-F. Shi, Dehydrogenation of methylcyclohexane over Pt-based catalysts supported on functional granular activated carbon, *RSC Adv.*, 2021, **11**, 29287–29297.
26 Y. Tuo, Y. Meng, C. Chen, D. Lin, X. Feng, Y. Pan, P. Li, D. Chen, Z. Liu, Y. Zhou and J. Zhang, Partial positively charged Pt in Pt/$MgAl_2O_4$ for enhanced dehydrogenation activity, *Appl. Catal., B*, 2021, **288**, 119996.
27 D. Zakgeym, T. Engl, Y. Mahayni, K. Müller, M. Wolf and P. Wasserscheid, Development of an efficient Pt/SiO_2 catalyst for the transfer hydrogenation from perhydro-dibenzyltoluene to acetone, *Appl. Catal., A*, 2022, **639**, 118644.
28 X. Wu, H. Lu, Y. Xiao, H. Guo, L. Jia and D. Li, Acid site introduced by Al^{3+}_{penta} and boron in Pt/Al_2O_3 catalyst for dehydrogenation of methylcyclohexane, *Int. J. Hydrogen Energy*, 2022, **47**, 34955–34962.
29 X. Yang, Y. Song, T. Cao, L. Wang, H. Song and W. Lin, The double tuning effect of TiO_2 on Pt catalyzed dehydrogenation of methylcyclohexane, *Mol. Catal.*, 2020, **492**, 110971.
30 R. Garidzirai, P. Modisha, I. Shuro, J. Visagie, P. van Helden and D. Bessarabov, The Effect of Mg and Zn Dopants on Pt/Al_2O_3 for the Dehydrogenation of Perhydrodibenzyltoluene, *Catalysts*, 2021, **11**, 490.
31 R. Garidzirai, P. Modisha and D. Bessarabov, Assessment of Reaction Kinetics for the Dehydrogenation of Perhydro-Dibenzyltoluene Using Mg- and Zn-Modified Pt/Al_2O_3 Catalysts, *Catalysts*, 2024, **14**, 32.
32 Y. Zhou, S. Qi, X. Tan, B. Yang and C. Yi, Regulating the Pt dispersion by increasing the specific surface area of Al_2O_3 support for perhydro-dibenzyltoluene catalytic dehydrogenation reaction, *Int. J. Hydrogen Energy*, 2024, **57**, 52–59.
33 L. Shi, Y. Zhou, X. Tan, S. Qi, K. J. Smith, C. Yi and B. Yang, The effects of alumina morphology and Pt electron property on reversible hydrogenation and dehydrogenation of dibenzyltoluene as a liquid organic hydrogen carrier, *Int. J. Hydrogen Energy*, 2022, **47**, 4704–4715.
34 Y. Yue, X. Liu, M. Shakouri, Y. Hu, Y. Guo and Y. Wang, Active and stable Pt-Ga_2O_3/Al_2O_3 catalyst for dehydrogenation of methylcyclohexane, *Catal. Today*, 2024, **433**, 114688.

35 Y. Jo, D. Kim, T. W. Kim, D. Yoon and Y.-W. Suh, Highly dispersed Pt–MnOx nanoclusters for the promoted activity of mesoporous Pt–MnO_x–Al_2O_3 in dehydrogenation of perhydro-benzyltoluene, *Appl. Catal., B*, 2023, **334**, 122848.

36 Y. Tuo, Y. Meng, Q. Lu, Q. Wang, F. Jia, Y. Zhou, X. Feng, J. Zhang, X. Duan and D. Chen, Taming Pt 5d state occupancy via Pt–O–Mn electronic linkage for enhanced dehydrogenation activity, *AIChE J.*, 2023, **69**, e18149.

37 A. de Oliveira, F. Lederle, P. Memmel, E. G. Hübner, P. Wasserscheid, M. Wolf and F. Auer, Pt–Re dehydrogenation catalysts synthesized via solvent deficient precipitation, *Catal. Sci. Technol.*, 2026, **16**, 2933–2945.

38 Y. Mahayni, L. Maurer, F. Auer, A. Hutzler, P. Wasserscheid and M. Wolf, Structure sensitivity of the low-temperature dehydrogenation of perhydro dibenzyltoluene on supported platinum nanoparticles, *Catal. Sci. Technol.*, 2024, **14**, 5464–5473.

39 Y. Mahayni, L. Maurer, I. Baumeister, F. Auer, P. Wasserscheid and M. Wolf, Batch and Continuous Synthesis of Well-Defined Pt/Al_2O_3 Catalysts for the Dehydrogenation of Homocyclic LOHCs, *ChemCatChem*, 2025, **17**, e202401762.

40 Y. Wu, Y. Li, X. Yu, X. Ma, M. Boebinger, J. Weber and Z. Wu, Insights into size effects of Pt/Al_2O_3 catalysts on hydrogen production from methylcyclohexane dehydrogenation, *Catal. Sci. Technol.*, 2024, **14**, 1791–1801.

41 M. Amende, C. Gleichweit, S. Schernich, O. Höfert, M. P. A. Lorenz, W. Zhao, M. Koch, K. Obesser, C. Papp, P. Wasserscheid, H.-P. Steinrück and J. Libuda, Size and Structure Effects Controlling the Stability of the Liquid Organic Hydrogen Carrier Dodecahydro-N-ethylcarbazole during Dehydrogenation over Pt Model Catalysts, *J. Phys. Chem. Lett.*, 2014, **5**, 1498–1504.

42 A. Ellert, F. Herold, M. Rønning, A. Hutzler, L. Piccirilli, T. V. W. Janssens, P. N. R. Vennestrøm, P. Wasserscheid and P. Schühle, Phosphorus-modification of Pt/Al_2O_3 catalysts improves dispersion and cycloalkane dehydrogenation activity, *J. Catal.*, 2024, **436**, 115607.

43 Y. Zhang, Z. Sheng, Q. Wang, J. Liu, H. Wei, Y. Xi, H. Hu, X. Feng and X. Lin, Effect of Sn on the perhydro-benzyltoluene dehydrogenation with the Sn-incorporated Pt/γ-Al_2O_3 catalyst, *Chin. J. Chem. Eng.*, 2026, **92**, 142–151.

44 K. Alconada and V. L. Barrio, Enhancing perhydrobenzyltoluene dehydrogenation performance with Co, Mo and Mn metal oxides: A comparative study with Pt/Al_2O_3 catalyst, *Appl. Catal., B*, 2024, **357**, 124349.

45 C. H. Kim, M.-W. Lee, J. S. Jang, S. H. Lee and K.-Y. Lee, Enhanced activity of a WO_x-incorporated Pt/Al_2O_3 catalyst for the dehydrogenation of homocyclic LOHCs: Effects of impregnation sequence on Pt–WO_x interactions, *Fuel*, 2022, **313**, 122654.

46 K. Murata, N. Kurimoto, Y. Yamamoto, A. Oda, J. Ohyama and A. Satsuma, Structure–Property Relationships of Pt–Sn Nanoparticles Supported on Al_2O_3 for the Dehydrogenation of Methylcyclohexane, *ACS Appl. Nano Mater.*, 2021, **4**, 4532–4541.

47 A. Ellert, F. Ding, A. Hutzler, F. Herold, L. Piccirilli, M. Rønning, T. V. W. Janssens, D. Wisser and P. Schühle, Solvent-free phosphorus modification of Pt/Al_2O_3 catalysts to improve dispersion and dehydrogenation activity, *Appl. Catal., A*, 2025, **696**, 120199.

48 D. Strauch, P. Weiner, B. B. Sarma, A. Körner, E. Herzinger, P. Wolf, A. Zimina, A. Hutzler, D. E. Doronkin, J.-D. Grunwaldt, P. Wasserscheid and M. Wolf, Bimetallic platinum rhenium catalyst for efficient low temperature dehydrogenation of perhydro benzyltoluene, *Catal. Sci. Technol.*, 2024, **14**, 1775–1790.

49 K. Alconada and V. L. Barrio, Evaluation of bimetallic Pt–Co and Pt–Ni catalysts in LOHC dehydrogenation, *Int. J. Hydrogen Energy*, 2024, **51**, 243–255.

50 Z. Peng, H. Lu, S. Zhang, X. Cao, J. Chen, B. Wei, M. Sang, H. Wang and Y. Sun, Pt–Sn Alloy Nanoparticles Supported on Al_2O_3 for the Dehydrogenation of Octadecahydro-dibenzyltoluene, *ACS Appl. Nano Mater.*, 2023, **6**, 16152–16160.

51 M. M. Distel, J. M. Margutti, J. Obermeier, A. Nuß, I. Baumeister, M. Hritsyshyna, A. Weiß and M. Neubert, Large-Scale H_2 Storage and Transport with Liquid Organic Hydrogen Carrier Technology: Insights into Current Project Developments and the Future Outlook, *Energy Technol.*, 2025, **13**, 2301042.

52 O. Levenspiel, *Chemical reaction engineering*, John Wiley & Sons, New York, 3rd edn, 1999.

53 G. Emig, E. Klemm and H. Freund, *Chemische Reaktionstechnik*, Springer Berlin Heidelberg, Berlin, Heidelberg, 2024.

54 M. Willer, P. Preuster, M. Geißelbrecht and P. Wasserscheid, Continuous dehydrogenation of perhydro benzyltoluene and perhydro dibenzyltoluene in a packed bed vertical tubular reactor – The role of LOHC evaporation, *Int. J. Hydrogen Energy*, 2024, **57**, 1513–1523.

55 E. Herzinger, J. Berger and M. Wolf, Continuous dehydrogenation of perhydro benzyltoluene in a three-phase stirred tank slurry reactor, *Chem. Eng. J.*, 2026, **534**, 175168.

56 T. Mader, M. Blasius, S. Pappler, T. Rüde, M. Geißelbrecht and P. Wasserscheid, Development of a kinetic approach for the liquid phase dehydrogenation of perhydro benzyltoluene, *Fuel*, 2026, **406**, 136928.

57 E. N. Bakatula, D. Richard, C. M. Neculita and G. J. Zagury, Determination of point of zero charge of natural organic materials, *Environ. Sci. Pollut. Res.*, 2018, **25**, 7823–7833.

58 S. Mustafa, B. Dilara, K. Nargis, A. Naeem and P. Shahida, Surface properties of the mixed oxides of iron and silica, *Colloids Surf., A*, 2002, **205**, 273–282.

59 T. Mahmood, M. T. Saddique, A. Naeem, P. Westerhoff, S. Mustafa and A. Alum, Comparison of Different Methods for the Point of Zero Charge Determination of NiO, *Ind. Eng. Chem. Res.*, 2011, **50**, 10017–10023.

60 G. Lauermann, P. Häussinger, R. Lohmüller and A. M. Watson, Hydrogen, 1. Properties and Occurrence, *Ullmann's Encyclopedia of Industrial Chemistry*, Wiley-VCH, Weinheim, 6th edn, 2003.

61 W. Reschetilowski, *Einführung in die Heterogene Katalyse*, Springer Berlin Heidelberg, Berlin, Heidelberg, 2015.

62 T. Prohaska, J. Irrgeher, J. Benefield, J. K. Böhlke, L. A. Chesson, T. B. Coplen, T. Ding, P. J. H. Dunn, M. Gröning, N. E. Holden, H. A. J. Meijer, H. Moossen, A. Possolo, Y. Takahashi, J. Vogl, T. Walczyk, J. Wang, M. E. Wieser, S. Yoneda, X.-K. Zhu and J. Meija, Standard atomic weights of the elements 2021 (IUPAC Technical Report), *Pure Appl. Chem.*, 2022, **94**, 573–600.

63 P. J. Mohr and B. N. Taylor, CODATA recommended values of the fundamental physical constants: 1998, *Rev. Mod. Phys.*, 2000, **72**, 351–495.

64 T. Rüde, Y. Lu, L. Anschütz, M. Blasius, M. Wolf, P. Preuster, P. Wasserscheid and M. Geißelbrecht, Performance of Continuous Hydrogen Production from Perhydro Benzyltoluene by Catalytic Distillation and Heat Integration Concepts with a Fuel Cell, *Energy Technol.*, 2023, **11**, 2201366.

65 A. Wunsch, M. Mohr and P. Pfeifer, Intensified LOHC-Dehydrogenation Using Multi-Stage Microstructures and Pd-Based Membranes, *Membranes*, 2018, **8**, 112.

66 A. Ali, A. K. Rohini and H. J. Lee, Dehydrogenation of perhydro-dibenzyltoluene for hydrogen production in a microchannel reactor, *Int. J. Hydrogen Energy*, 2022, **47**, 20905–20914.

67 I. S. Lim, Y. Jeong, Y. Kwak, E.-R. On, Q. N. Dao, H. Jeong, H. Sohn, S. W. Nam, T.-H. Lim, K. Müller and Y. Kim, Maximizing clean hydrogen release from perhydro-benzyltoluene: Energy-efficient scale-up strategies and techno-economic analyses, *Chem. Eng. J.*, 2023, **478**, 147296.

68 F. Florit, V. Busini and R. Rota, Kinetics-free process intensification: From semi-batch to series of continuous chemical reactors, *Chem. Eng. Process.*, 2020, **154**, 108014.

69 F. Maestri, S. Copelli, M. Barozzi and R. Rota, Kinetic-free discontinuous to continuous transformation of fine chemical reactions: A general experimental procedure, *Chem. Eng. J.*, 2020, **395**, 125061.

70 S. Copelli, M. Barozzi, F. Maestri and R. Rota, Safe optimization of potentially runaway reactions: From fedbatch to continuous stirred tank type reactor, *J. Loss Prev. Process Ind.*, 2018, **55**, 289–302.

71 B. W. Brooks, Product yields from the Van de Vusse reaction scheme: use of semi-batch reactors, *Chem. Eng. Sci.*, 1990, **45**, 1589–1594.

72 S. Mehdiabadi, J. B. P. Soares and A. H. Dekmezian, Production of Long-Chain Branched Polyolefins with Two Single-Site Catalysts: Comparing CSTR and Semi-Batch Performance, *Macromol. React. Eng.*, 2008, **2**, 529–550.

73 R. W. Chylla, J. D. Campbell and F. Teymour, Dynamics of semibatch polymerization reactors: II. Pilot-plant study, *AIChE J.*, 1997, **43**, 157–165.

74 S. Rohani and J. Baldyga, Micromixing described in terms of inertial-convective disintegration of large eddies and viscous-convective interactions among small eddies – II. Semi-batch and continuous stirred tank reactors, *Chem. Eng. Sci.*, 1987, **42**, 2611–2619.

75 *Handbook of heterogeneous catalysis*, ed. G. Ertl, H. Knözinger, F. Schüth and J. Weitkamp, Wiley-VCH, Weinheim, 2nd edn, 2008.

76 M. Willer, P. Preuster, P. Malgaretti, J. Harting and P. Wasserscheid, Heat transfer to a catalytic multiphase dehydrogenation reactor, *Int. J. Hydrogen Energy*, 2024, **80**, 1011–1020.

77 N. Szesni, F. Frankl, S. Sturm, P. Wasserscheid, A. Seidel and A. Boesmann, *US Pat.*, US12269018B2, 2025.